Acoustic emission sensing as a tool for understanding the mechanisms of abrasive water jet drilling of difficult-to-machine materials

R Kovacevic[1]*, **H-S Kwak**[1]** and **R S Mohan**[2]
[1]Department of Mechanical Engineering, University of Kentucky, Lexington, Kentucky, USA
[2]Department of Mechanical Engineering, University of Tulsa, Oklahoma, USA

Abstract: For drilling difficult-to-machine materials, abrasive water jet (AWJ) drilling provides several advantages not offered by other machining methods, such as the capability to achieve higher depth–diameter ratios, the absence of a heat-affected zone, and no thermal distortion. An acoustic emission (AE) sensing technique is used to study the material removal mechanisms involved in the AWJ drilling process. The feasibility of using r.m.s. acoustic emission (AE_{RMS}) to monitor the AWJ drilling depth on-line is also investigated. Stochastic modelling of the time domain AE signal provides more insight into the physics of the process.

Keywords: acoustic emission, abrasive water jet, ceramics, stochastic modelling, erosion

NOTATION

a	time constant
a_t	random noise (white noise)
d_i	variance decomposition
f	normalized frequency
f_b	break frequency
f_d	damped natural frequency
g_i	Green's function
h	drilling depth
h_{max}	theoretically maximum possible drilling depth
p,q	order of ARMA model
$p(f)$	power spectrum density function
t	time
x	$Re(\lambda_i)$
y	$Im(\lambda_i)$
y_t	amplitude of AE signal
z	real root of ARMA model
γ_0	auto-covariance function
δ	sampling length
$\theta_1, \ldots, \theta_q$	moving average coefficients
λ_i	characteristic roots of ARMA model
σ_a^2	variance of white noise
$\phi_1, \ldots, \phi_p$	auto-regressive coefficients

The MS was received on 3 June 1996 and was accepted for publication on 4 August 1997.
**Present address: Southern Methodist University, Dallas, Texas, USA.*
***Present address: LG-EDS Systems Inc., Seoul, South Korea.*

1 INTRODUCTION

Since its introduction in 1983 as a commercial system for cutting glass, abrasive water jet (AWJ) machining has been used increasingly as a versatile tool for contour cutting, milling and drilling applications. For cutting difficult-to-machine materials AWJ offers the two unique advantages of no heat-affected zone and no thermal distortion. Hence, materials such as glass, titanium, super-alloys, metal–matrix composites and ceramics are frequently cut with AWJ. Even though there have been several investigations in the area of AWJ cutting (**1**), only a few studies (**2**–**6**) have addressed the AWJ drilling process. Therefore, there remains a need to study the AWJ drilling process in order to understand better the mechanisms involved.

Drilling difficult-to-machine materials with solid drill bits is often not possible owing to the non-homogeneous nature of the materials and their unpredictable response to the drill bit action. Although lasers are often used for drilling these materials, the use of lasers results in undesirable surface characteristics, considerable heating of the work piece and the need for additional processing (**7**), which significantly increase the cost of machining. Lasers and solid drill bits can only produce holes having relatively small depth–diameter ratios. Among the various machining techniques, AWJ drilling, which can provide large depth–diameter ratios, has shown promise for machining these materials owing to the advantages mentioned above.

Critical process parameters that influence an AWJ drilling operation are stand-off distance, pump pressure,

abrasive flowrate, abrasive material and grain size, the back flow of water, jet impact angle and drilling time. Control of hole geometry and hole quality can be achieved by varying stand-off distance, abrasive flowrate, abrasive material and abrasive size, whereas drilling depth can be controlled by varying pump pressure, jet impact angle and drilling time. Apart from these parameters, drilling performance in terms of material removal rate or penetration rate is influenced by the material properties and back flow of the jet from the bottom of the hole. The back flow of the rebounded jet causes turbulence inside the drilled hole, reduces the particle velocity and interferes with the drilling process.

Hashish (**2**) investigated AWJ drilling of glass and laminated composites and found that low pressures (about 30–40 MPa) should be used for glass piercing. High-pressure piercing resulted in fracture or cracking owing to the shock loading of water or hole hydrodynamic pressurization. An AWJ rock drill has been developed by Savanick and Krawza (**3**) and Hashish (**4**) for drilling quartzite with compressive strengths as high as 503 MPa. The investigators suggested that rotary dual (or multiple) drilling is the most promising technique as it is capable of generating high-efficiency jets at optimum mixing conditions. Using an open-loop approach, Hashish and Whalen (**5**) attempted to control hole quality and hole size through pressure ramping in precision drilling of ceramic coated components. However, a closed-loop control system with an automatic in-process hole size sensor is still needed. Raju and Ramulu (**6**) have reported a semi-empirical transient numerical model for predicting the depth of AWJ drilling, but the experimental results did not closely match the model predictions, especially for extremely low or high drilling depths.

Depth monitoring in opaque materials during AWJ drilling of small diameter holes is very difficult to perform without interruptions. Without suitable monitoring methods, it is not possible to efficiently control the drilling process. From a process efficiency point of view, interrupting the drilling process to monitor the depth is not a feasible approach. Hence, there is an increasing need to develop a suitable indirect monitoring technique for the hole depth in an AWJ drilling operation. In the field of abrasive water jet cutting technology, Mohan *et al.* (**8**) have applied acoustic emission (AE) techniques for monitoring depth of cut in grey cast iron. They found that the power spectrum density of the autoregressive moving average (ARMA) model representing the time domain AE signals gave a good indication of the depth of penetration. Thus AE sensing could be considered as a promising technique for depth monitoring in the AWJ drilling process also.

Recently, AE sensing has been widely used for monitoring manufacturing processes (**9**–**11**). Liu and Dornfeld (**9**) used AE_{RMS} as an indicator of depth of cut in precision machining operations such as single point diamond turning. AE_{RMS} was a good source of information to predict the cutting mechanisms in micromachining (**9**). Tool wear in milling operations (**12**) and grinding wheel wear (**13**) have also been monitored using AE signals. Pandit and Stacey (**13**) proposed using data dependent system analysis for correlating the AE modes with different cutting conditions such as depth of cut, grinding wheel grade, cutting speed or type of work piece material. The AE technique has also been used for in-process control of laser drilling (**14**) through depth regulation and beam breakthrough control. AE measurements of brittle materials (**15**) during AWJ cutting have shown that a link exists between the modes of the AE signal and the material removal mechanisms.

The investigations discussed above suggest that AE might be a promising tool for sensing manufacturing processes and understanding the underlying mechanisms involved. The literature survey also indicates that there has been little work done towards understanding the mechanisms involved in the AWJ drilling process. Moreover, a suitable strategy needs to be developed to monitor on-line the depth of drilling in opaque materials. The current investigation is aimed at determining the feasibility of using the AE sensing technique as a tool for monitoring AWJ drilling of ceramic materials. Stochastic modelling of the time domain AE signal provides relevant and useful information about material removal mechanisms in the drilling process. This paper investigates the AWJ drilling of a stationary workpiece with a stationary jet.

2 EXPERIMENTAL SET-UP AND PROCEDURE

The experimental set-up consists of an AWJ system, AE sensor, signal processor and workpieces. The AWJ system used for performing the experiments consists of a high-pressure intensifier pump, AWJ cutting head, abrasive metering and delivery system, abrasive hopper with garnet as abrasive, catcher tank and X–Y–Z positioning system controlled by a CNC (computer numerical controller). A schematic diagram of the experimental set-up is shown in Fig. 1a. Figure 1b shows the cross-section of a hole drilled with AWJ, indicating the impinging jet and the rebounded jet. The generated AE signals were detected and processed by a Model AET 5500 acoustic emission monitoring system which consists basically of an AET 5500 mainframe (signal processing unit with amplifier), graphics terminal (interface, data storage and display) and the accessories (sensors and pre-amplifier). When acoustic emission caused by an induced stress occurs in a test specimen, the sensors (resonant frequency 2 MHz) convert this AE wave into a voltage signal which is amplified by the pre-amplifier and is sent to the amplifier in the mainframe (16-bit microprocessor) for post-processing. For detecting the AE signals from the AWJ drilling process, a sensor was fixed on the side wall of the workpieces with a water-resistant epoxy gum. Three types of non-homogeneous refractory ceramics, namely magnesia chromite, sintered magnesia and bauxite of 51 mm thickness, were used for this investigation. The workpiece material properties and their compositions are given in Table 1. A pencil-lead break test was performed for each trial to ensure proper connection and attachment

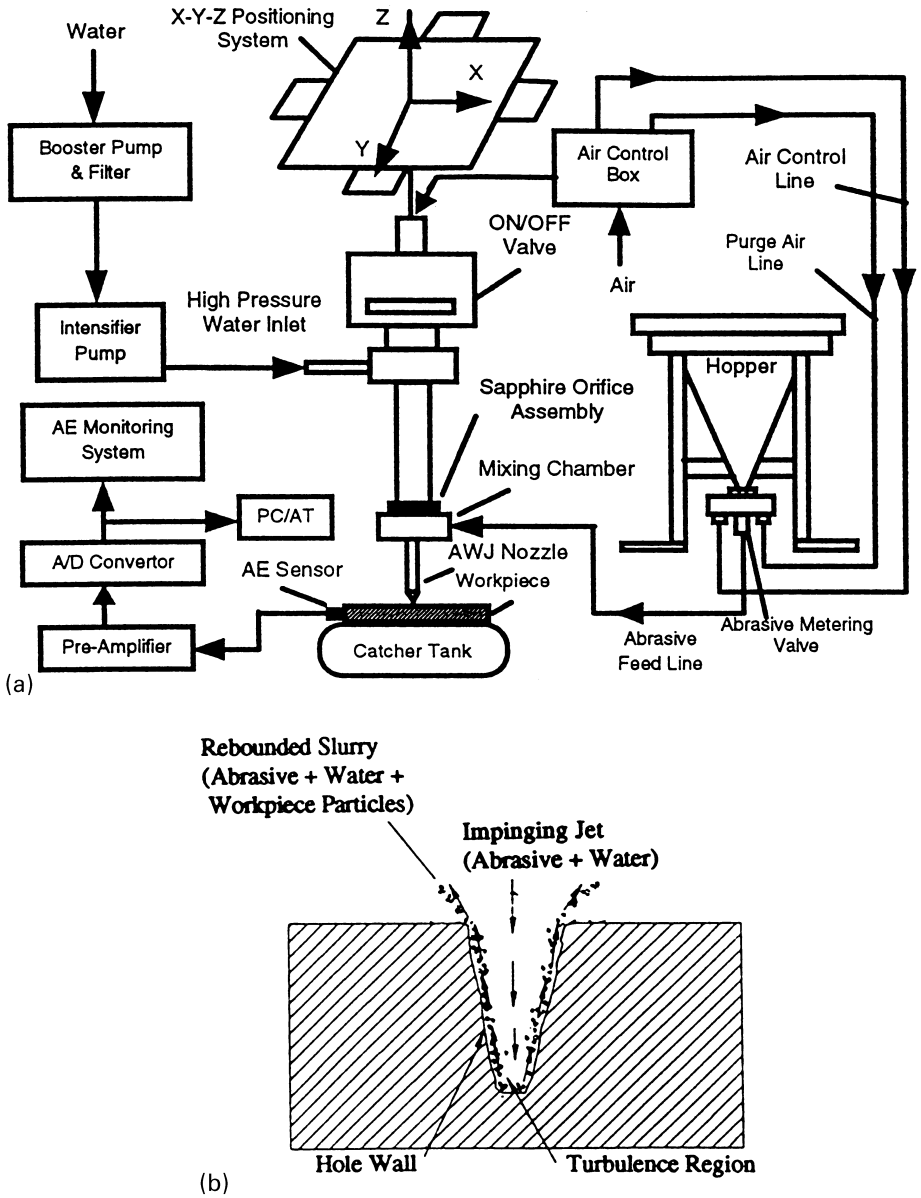

Fig. 1 (a) Experimental set-up; (b) typical cross-section of a drilled hole

of the sensor. Holes of different depths were drilled in the workpiece using the same set of process parameters, given in Table 2.

AE signals were acquired at a sampling frequency of 1 MHz (at a pre-amplifier gain of 100.0 and amplifier gain of 5.0) with progressive drilling time. Signals were monitored during three stages of the drilling process, namely the pure water impingement stage, the drilling stage, where

Table 1 Workpiece material properties

Material	Density (g/cm^3)	Porosity (%)	Cold compressive strength (MPa)	Cold bend, tensile strength (MPa)	Young's modulus (MPa)	Composition (%)
Magnesia chromite	3.26	15.20	30.00	3.50	13 000.00	Al_2O_3-6, Fe_2O_3-14, SiO_2-0.5, MgO-60, CaO-1.3, Cr_2O_3-18
Sintered magnesia	3.00	15.20	40.00	14.00	85 000.00	Al_2O_3-0.1, Fe_2O_3-0.2, SiO_2-0.5, MgO-97, CaO-2.1
Bauxite	2.89	15.00	126.00	19.00	59 000.00	Al_2O_3-81, Fe_2O_3-1.7, SiO_2-12, CaO + MgO-0.4, TiO_2-3.2, $K_2O + Na_2O$-1.8

Table 2 Process parameters

Parameter	Value
Abrasive material	Garnet
Abrasive mesh size	80
Abrasive particle shape	Angular (random)
AWJ orifice material	Sapphire
AWJ orifice diameter	0.46 mm
Mixing nozzle diameter	1.27 mm
Mixing nozzle length	88.9 mm
Method of feed	Suction
Condition of abrasive	Dry
Angle of jet	90°
Material thickness	51 mm
Pump pressure	206 MPa
Abrasive flowrate	5.75 g/s
Stand-off distance	5 mm
Materials	Magnesia chromite, sintered magnesia, bauxite

the target material is subjected to erosion by abrasive water jet mixture, and the dwell stage, which occurs after full penetration of the target material. The time domain AE signal was acquired in several data sets over the entire drilling process. Each data set consisted of 1024 data points representing the AE signal generated at a particular instant of time. The fast Fourier transform (FFT) of the time domain signal was calculated and the average of five FFT readings of signals belonging to the same process stage were determined for further analysis. Stochastic modelling of the time domain signals was performed through the ARMA modelling technique. Several holes of different depths were also drilled and the time taken was noted in order to determine the material removal rate and the penetration rate. Each drilled hole was filled with fine abrasive particles. The volume occupied by the abrasive particles is multiplied by the density of the workpiece material to determine the weight of the material removed, which when divided by the drilling time yielded the material removal rate. The penetration rate is determined from the ratio of the depth of the drilled hole and the time taken. All these experiments were performed five times using the same set of process parameters and workpiece material to verify the repeatability of the results.

3 RESULTS AND DISCUSSION

Initial investigations were conducted to evaluate the drilling performance by monitoring the depth of penetration, penetration rate and material removal rate. The results of this investigation are presented below, beginning with a brief discussion of the characteristics of the AE signal. Discussion on the strategy of monitoring drilling depth through the AE sensing technique is presented in Section 3.3. This is followed by Section 3.4 in which the results of the time series modelling technique and the information they provide about the physics of the process are briefly discussed.

3.1 Acoustic emission sensing

Acoustic emission, also called stress wave emission, is produced by microscopic deformations occurring in materials as they are stressed. It contains part of the elastic energy released during deformation. Acoustic emission is associated with dislocation movements, crack growth, deformation of inclusions and with other mechanisms. These sources are clearly present in AWJ machining. Other AE sources arise from the fluid dynamics of the AWJ process such as turbulence and cavitation. The characteristics of the AE signal generated during the machining process depend on the source of generation and the material properties. Acoustic emission signals generally can be classified into continuous and burst type. Continuous-type AE signals are associated with plastic deformation in ductile materials and erosion processes in brittle materials (**15**), while burst-type signals are observed in unsteady processes such as cracking in materials (**16**), transgranular spalling fracture (**15**) and cavitation. However, it must be noted that at any instant of time there could be more than one source generating the AE signal and hence the general characteristics of the signal are determined by the dominant source. Information about the dominant source can be obtained through several means such as identification of the type of AE signal and frequency decomposition of the ARMA model representing the time domain signal.

The most frequently used AE signal parameters for investigations are peak amplitude, rise time, event counts and event duration. These parameters have been used for monitoring tool wear and tool breakage, fracture mechanisms and process condition monitoring. Other features contained in the raw AE signal are energy, spectrum distribution and amplitude distribution. The first one can be represented by the r.m.s. voltage, the second one is reflected in the zero crossing rate and the last one will be reflected in the skewness and kurtosis of the AE signal.

Typical time domain AE signals and their corresponding FFTs for different stages of the drilling process and for materials of different mechanical properties are shown in Figs 2 and 3 respectively. It can be seen that the amplitude for the pure water impingement stage is about three to four times higher than for the drilling stage. It should also be noted that the amplitude corresponding to magnesia chromite in the pure water stage is lower than those of sintered magnesia and bauxite. When a pure water jet impinges on the workpiece, part of the energy is used for penetration (if the material properties allow it to happen) and part of the energy is lost in the fluid damping phenomena owing to factors such as turbulence and cavitation. As penetration depth increases, the effect of damping and the amount of energy dissipated also increase. For all the three materials investigated, the pure water jet penetrates less and hence less energy is dissipated in the material removal as well as in damping. As a result, almost the entire energy of the impinging jet is transmitted to the sensor through the workpiece in the form of vibrations. This could be the reason for

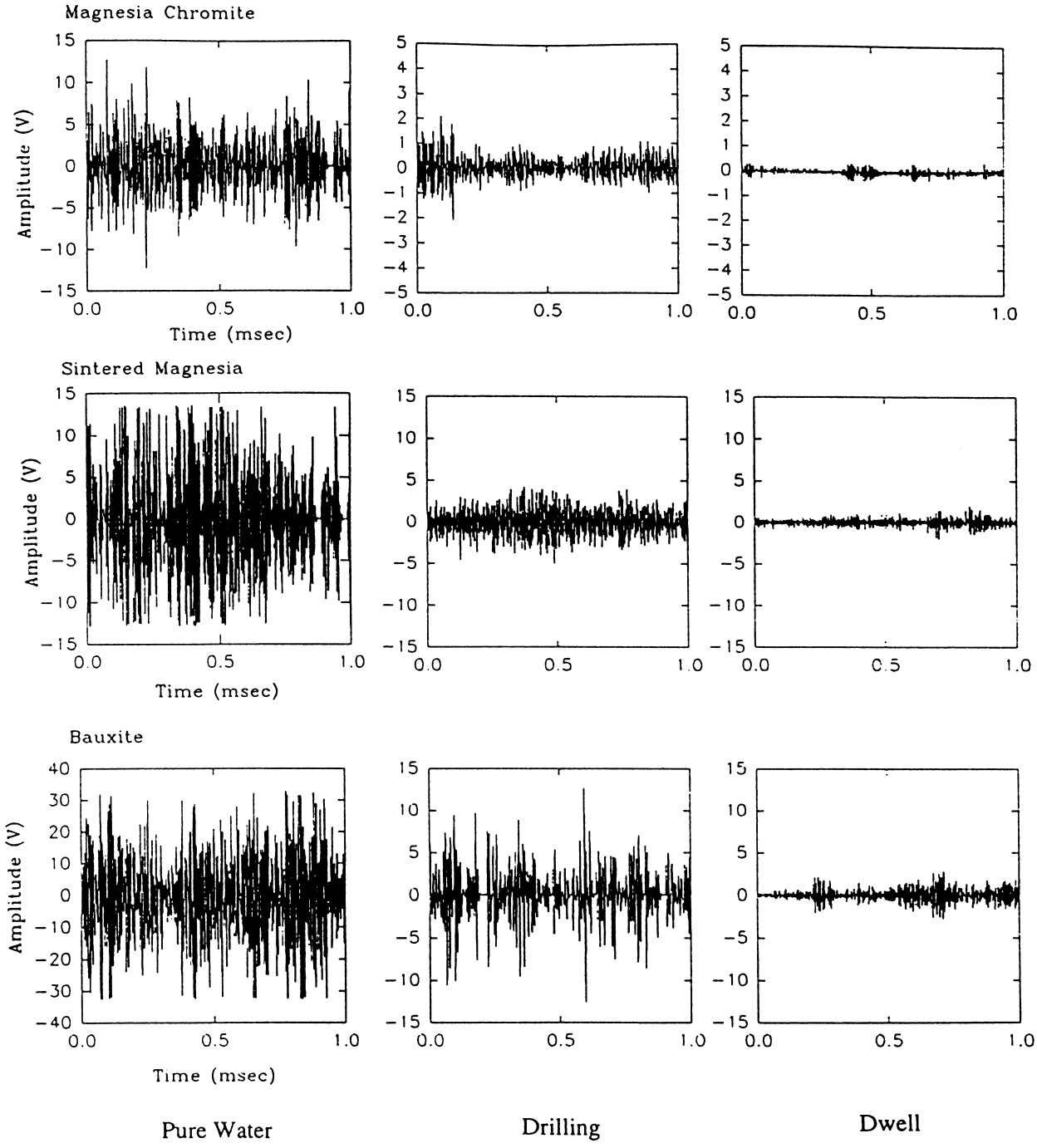

Fig. 2 Typical time domain AE signals for different process stages

the higher amplitude of the AE signal for pure water jet conditions. As noted above, for the case of bauxite, less energy is dissipated during the material removal process when the workpiece is impinged on by a pure water jet owing to the lower penetration. This is the reason for the relatively higher amplitude of the AE signal for bauxite.

The AE signal during the drilling stage is generated predominantly by phenomena related to the target material such as erosion, crack generation, crack propagation and turbulence. The AE signal in bauxite is primarily of the burst type, indicating a material removal mode due to trans-granular fracture, which is usually observed in comparatively high strength materials. Visual observation of the kerf wall of AWJ cutting of this material discussed in Section 3.4 supports this observation. The other materials show continuous-type signals which indicate a material removal mechanism caused by intergranular erosion or microcracking. It is not easy to predict the AE response owing to the non-homogeneous nature of the material, i.e. the presence of hard inclusions in a softer matrix. These

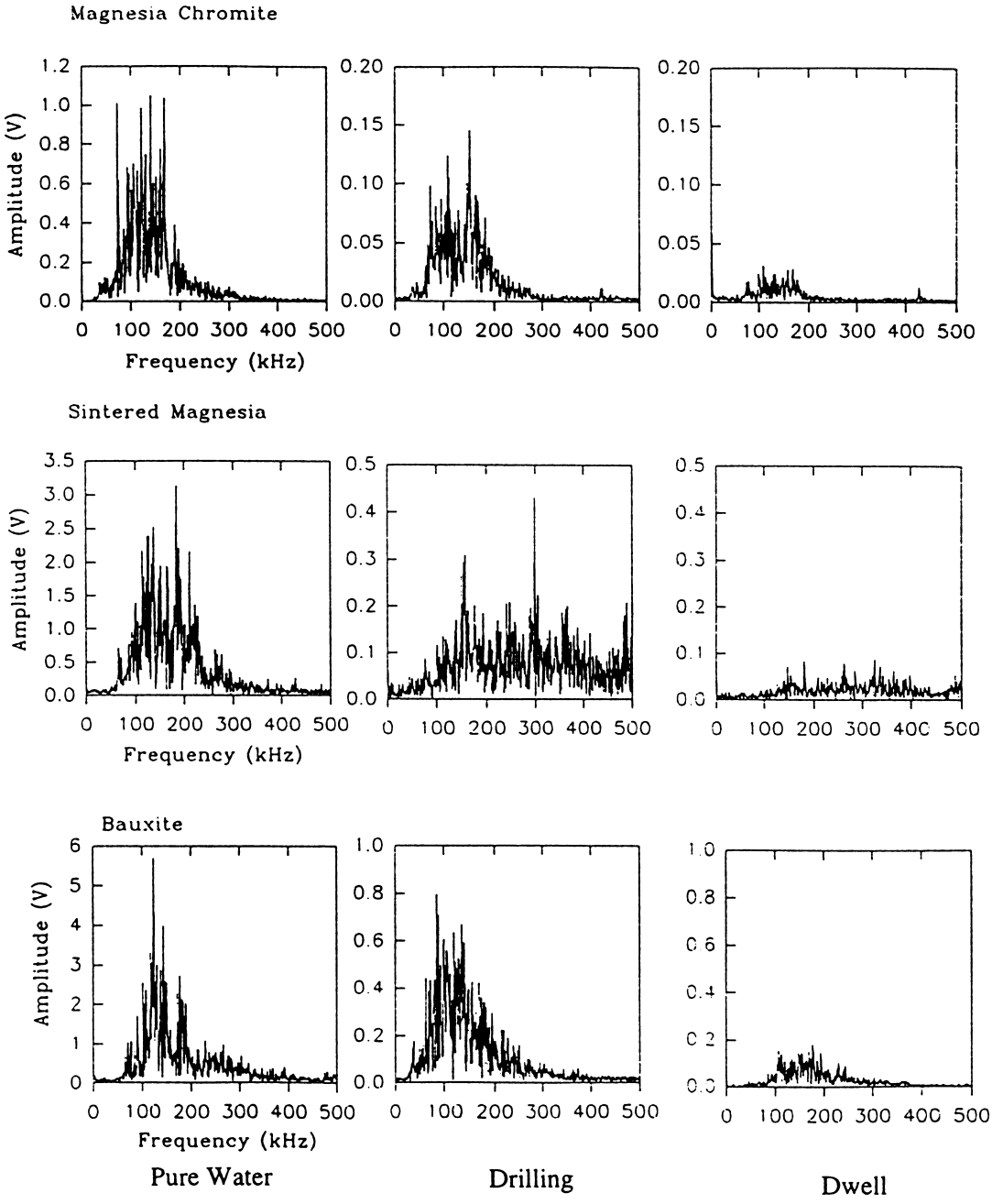

Fig. 3 Typical frequency domain AE signals for different process stages

aspects are discussed in detail in Section 3.4. It is observed from FFT graphs (Fig. 3) that for magnesia chromite and bauxite, the frequencies are concentrated between 70 and 170 kHz during the drilling stage. An AE signal with the frequency response concentrated in a narrow frequency range (in the case of bauxite) supports the previous observation that material removal occurs owing to transgranular fracture. However, frequencies in sintered magnesia are spread between 100 and 500 kHz which could be owing to material removal caused by an unsteady process such as continuous generation of a microcrack network. A continuous emission time domain AE signal with narrow frequency response observed in the case of magnesia chromite is indicative of material removal due to intergranular erosion. In all cases, a weak AE signal is detected after penetration (dwell stage) owing to AWJ impact on the hole wall surface. It may also be noted that dwell time is an important factor that affects the hole geometry and hole quality.

The results of the drilling performance evaluation studies are given in the next section followed by a brief discussion.

3.2 Drilling performance

Material removal rate, defined as the mass of material removed per unit time, was measured for each ceramic material with progressive drilling time and is indicated in

Fig. 4. It can be noted that the material removal rate does not change much with drilling time. As the drilling is performed by a stationary jet on a stationary workpiece, the jet continuously removes the workpiece material from the drilled hole and the removed material is displaced by jet back flow (see Fig. 1b). The newly exposed workpiece material in the hole is subjected to fresh AWJ mixture impingement. As a result, the local energy of the impinging jet is almost the same throughout the drilling depth. This could be the reason for the near constant material removal rate with progressive drilling time. As the compressive strength of the material increases, the material removal rate reduces as a result of the higher resistance of the target material. It is interesting to compare the material removal rate of the materials under study with the penetration rate during the AWJ drilling process. Figure 5 gives a plot of penetration rate for each material with progressive drilling time. Similar to the material removal rate, the penetration rate is also lower for materials with higher compressive strength. However, as time increases, the penetration rate reduces, as indicated by the respective quadratic equations. This could be due to the effect of the back flow of the jet which reduces the particle velocity and interferes with the impact process. The trends shown by Figs 4 and 5 suggest that, with progressive time, the AWJ mixture removes more material from the walls of the hole and less from the hole bottom, producing a diverging hole. This also supports the view that the back flow of the jet has sufficient kinetic energy to remove material in the above ceramics.

Investigations conducted by Hashish (**2**) on drilling of glass and lucite indicated that the penetration rate decreases significantly as depth increases. The semi-empirical transient numerical model suggested by Raju and Ramulu (**6**) for prediction of drilling depth was verified experimentally using transparent polycarbonate material, but the results did

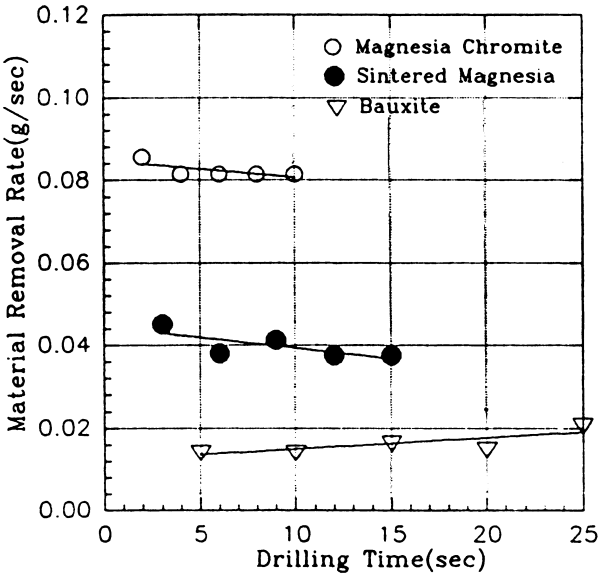

Fig. 4 Material removal rate for different ceramic materials

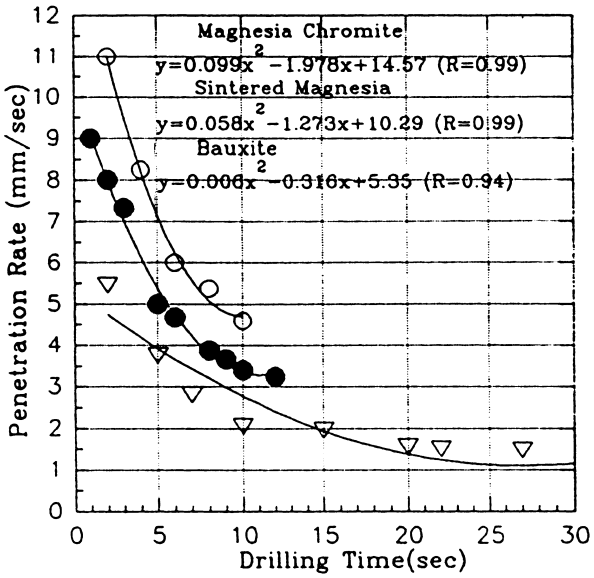

Fig. 5 Penetration rate for different ceramic materials

not show close conformance especially at low or high drilling depths. An attempt is made in the current investigation to determine a suitable empirical relationship between drilling depth and drilling time. Figure 6 shows the plots of the drilling depth versus drilling time for different materials. The trend exhibited by the data points was fitted better by an exponential relationship given by

$$h = h_{\max}[1 - \exp(-at)] \tag{1}$$

where, $h_{\max}$ is the theoretically maximum possible drilling depth and a is the time constant. It may be noted that $h_{\max}$ depends on the process parameters, mechanical properties of the material and material removal mechanisms. The time constant a depends on the compressive strength of ceramic materials. The higher the compressive strength, the lower the time constant becomes. The above exponential relationship is indicative of less efficient material penetration at larger depths. This is primarily due to the damping effect of the jet back flow. Similar results obtained by Hashish (**2**) and Raju and Ramulu (**6**) for other materials indicate that the above trend is primarily a feature of the AWJ drilling process.

3.3 Monitoring drilling depth

A plot of AE_{RMS} against drilling time is given in Fig. 7. AE_{RMS} decreases as the drilling time increases. Small diameter hole drilling has damping effects on the generated AE signal due to the presence of turbulence caused by the back flow of water. Damping effects increase in deeper holes because more abrasives, water and debris collect in the cavity. This could be the reason for the decrease in amplitude of the AE signal for higher drilling depths. Compared to magnesia chromite, bauxite has more variance in

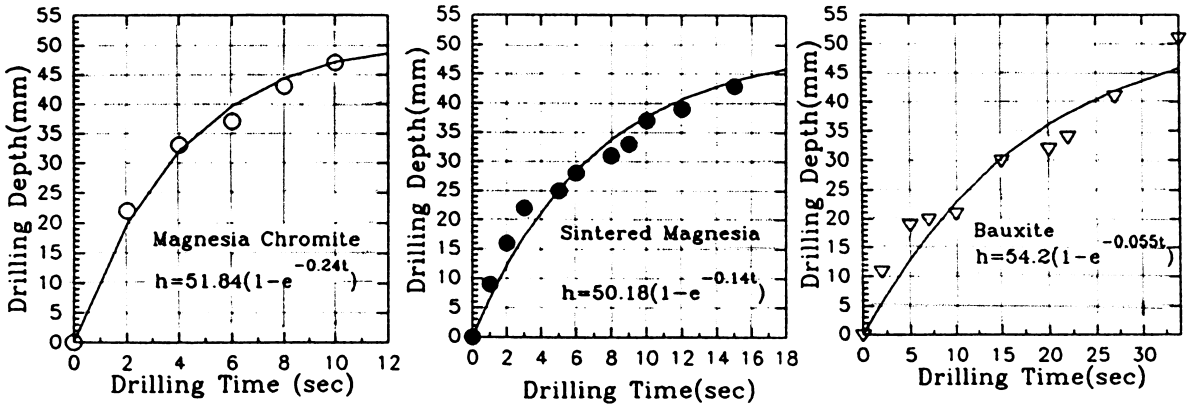

Fig. 6 Drilling depth versus drilling time

AE_{RMS}. This could be due to the presence of more hard inclusions. This trend in AE_{RMS} for all the three materials with progressive time indicates that AE_{RMS} can be effectively used for monitoring drilling depth.

Figure 8 shows plots of AE_{RMS} values against drilling depth for the three materials. Generally, the AE_{RMS} reduces with increase in drilling depth. This trend can be attributed to two causes, i.e. the non-linear trend of drilling depth with drilling time and the damping effect on the AE signal caused by AWJ debris present in the small diameter hole. The data of AE_{RMS} during the drilling stage were fitted using linear regression. An excellent fit to the data was achieved with R values of 0.98, 0.89 and 0.93 respectively. Higher variance in AE_{RMS} readings was observed for bauxite ceramic material which could be due to the presence of hard inclusions as noted earlier. It is interesting to note that the slope of the line relating AE_{RMS} and drilling depth is relatively low for sintered magnesia compared to the other two materials. This needs further investigation. AE_{RMS} is observed to be higher for materials of higher compressive strength for the same drilling time, which is due to more energy dissipation during the material removal process. The above trend in AE_{RMS} with drilling depth indicates that acoustic emission is a promising tool for on-line monitoring of AWJ drilling depth.

3.4 ARMA modelling

The raw signal from the AE monitoring system was acquired separately using a suitable PC based data acquisition system at a sampling frequency of 1 MHz for stochastic modelling and spectrum analysis. The time domain signal consisting of 1024 observations was analyzed using the ARMA modelling technique. The ARMA(p,q) model can

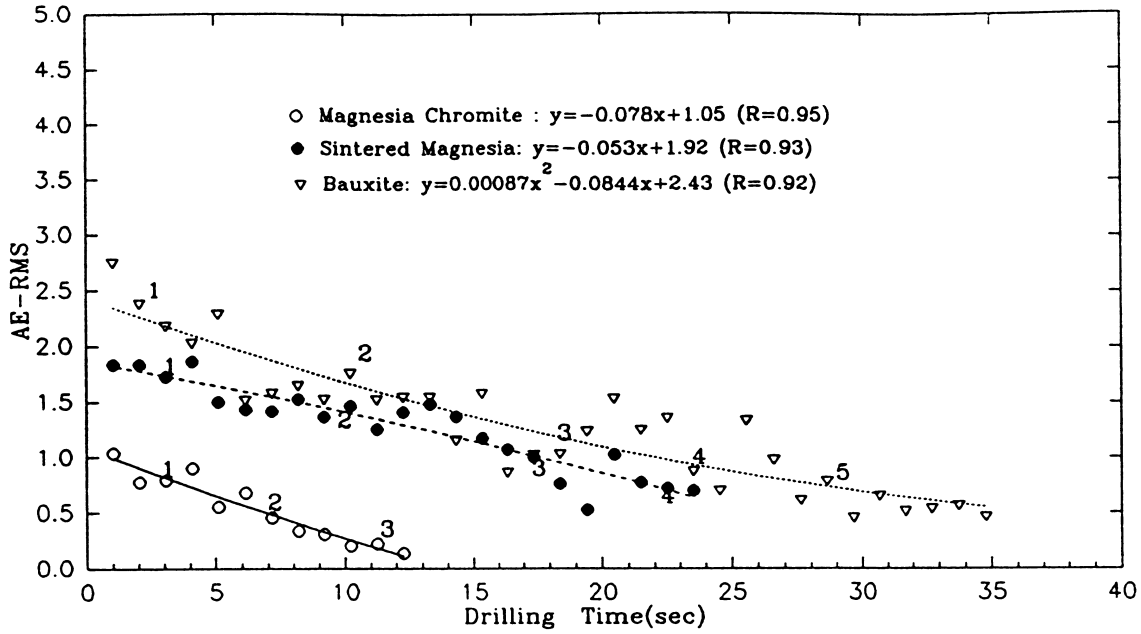

Fig. 7 AE_{RMS} versus drilling time

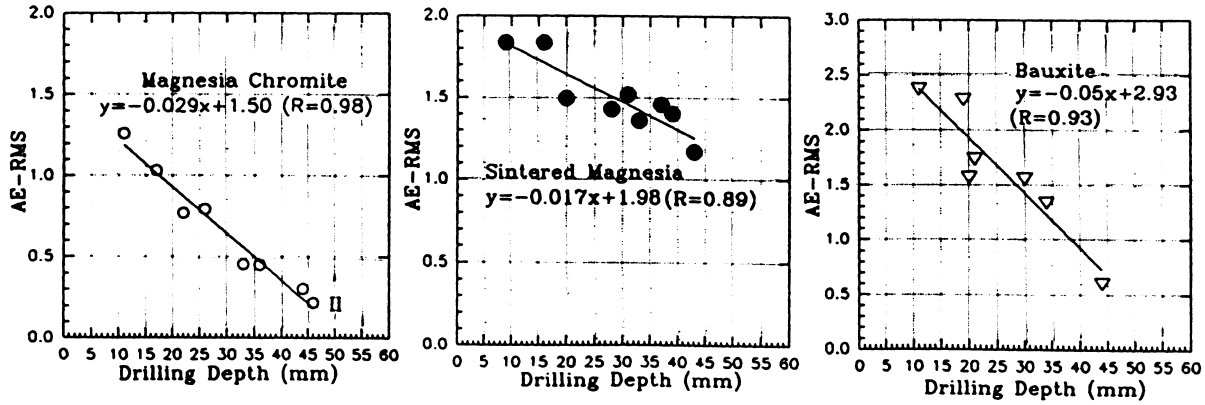

Fig. 8 AE_{RMS} versus drilling depth

be represented by the equation

$$Y_t - \phi_1 Y_{t-1} - \phi_2 Y_{t-2} - \cdots - \phi_p Y_{t-p} = a_t - \theta_1 a_{t-1} - \theta_2 a_{t-2} - \cdots - \theta_q a_{t-q} \quad (2)$$

where Y_t is the amplitude of the signal at time t, a_t is the white noise and $a_t \sim$ NID (0, σ_a^2). The orders of the best-fit ARMA models determined using the model distance approach (**17**) ranged from ARMA (6,5) to ARMA (2,1).

The power spectrum density (PSD) function of the ARMA(p,q) model, which is the transform of the auto covariance function, is given (**18**) by the equation

$$p(f) = 2\sigma_a^2 \frac{|1 - \theta_1 e^{-i2\pi f} - \theta_2 e^{-i4\pi f} - \cdots - \theta_q e^{-i2\pi qf}|^2}{\gamma_0 |1 - \phi_1 e^{-i2\pi f} - \phi_2 e^{-i4\pi f} - \cdots - \phi_p e^{-i2\pi pf}|^2} \quad (3)$$

where

$$0 \leqslant f \leqslant \frac{1}{2}, \qquad \gamma_0 = \sum_{i=1}^{p} d_i, \qquad d_i = \sum_{j=1}^{p} \frac{g_i g_j}{1 - \lambda_i \lambda_j}$$

The λ values are the characteristic roots of the ARMA model and g_i is given by

$$g_i = \frac{(\lambda_i^{p-1} - \theta_1 \lambda_i^{p-2} - \cdots - \theta_q)}{(\lambda_i - \lambda_1)(\lambda_i - \lambda_2) \cdots (\lambda_i - \lambda_{i-1})(\lambda_i - \lambda_{i+1}) \cdots (\lambda_i - \lambda_p)} \quad (4)$$

It may be noted that variance decomposition (d_i) of each root gives the relative power of the root. The power spectrum density of the best-fit ARMA model was obtained for further analysis.

The frequency decomposition of the roots of the ARMA(p,q) model can be derived (**19**) from each complex root, for instance $\lambda_{1,2} = x \pm iy$. It has a damped natural frequency given by

$$f_d = \frac{1}{2\pi\delta} \arccos\left[\frac{x}{\sqrt{(x^2 + y^2)}}\right] \quad (5)$$

where δ is the sampling length in seconds.

To distinguish between different real roots which contribute separately to the concentration of frequencies around zero, a pseudo frequency called the break frequency, corresponding to the half power point, was obtained for each real root. The break frequency of a real root, for example $\lambda_3 = z$, is given by

$$f_b = \frac{-\ln |z|}{2\pi\delta} \quad (6)$$

Even though FFT and PSD represent the power of the AE signal, the FFT was derived from the time domain data whereas the PSD was derived from the ARMA model representing the time domain data. The area under the PSD curve can be considered as a better representative of the power of the AE signal as it is devoid of white noise. Figures 9, 10 and 11 show the plots of PSD area against drilling time for magnesia chromite, sintered magnesia and bauxite respectively. It can be seen that magnesia chromite and sintered magnesia have two separately identified linear regions, whereas bauxite has three linear regions. Regions I and II of Figs 9, 10 and 11 match very closely with the trend of penetration rate. As with region I, the penetration rate has a steep decreasing initial trend until a particular depth, namely the critical depth, is reached, followed by a shallow trend corresponding to region II. This indicates that the area under the PSD curve is capable of providing information about the penetration process. The critical depths are marked in the respective figures. It may be noted that the instant at which the AE behaviour changes (indicated by the critical depth) occurs approximately after 22 per cent of the drilling time for all three materials. The critical depth is higher for materials with a lower compressive strength. In these materials, until the critical depth is reached the damping effect of the rebounded jet is not significant. However, after the critical depth, the trend becomes more shallow owing to the increased damping effect of the rebounded jet. The mechanisms related to the critical depth needs further investigation.

The three regions of bauxite material are discussed next in detail. In order to better understand the material removal

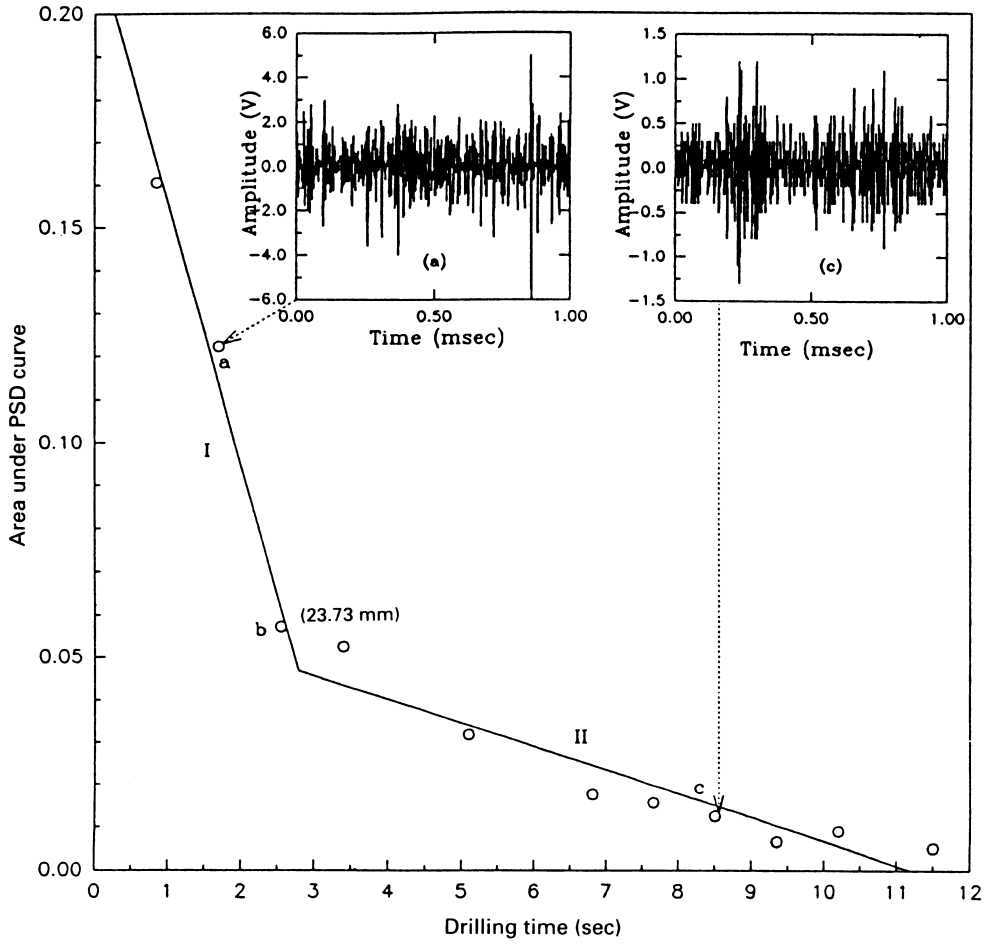

Fig. 9 Area under PSD curve versus drilling time (magnesia chromite)

mechanisms in the three materials, time domain signals representing each region have been plotted separately and are embedded in Figs 9, 10 and 11. It can be noted from Fig. 9 that the time domain AE signals corresponding to magnesia chromite material are of continuous type representing a material removal mechanism due to intergranular erosion or microcracking. In magnesia chromite, which is characterized by a lower Young's modulus and lower cold compressive strength, the presence of hard inclusions in a much softer matrix contribute to a material removal mechanism of intergranular erosion.

Similar to magnesia chromite, time domain signals of sintered magnesia shown in Fig. 10 are also of continuous type, but of much higher frequency. The high Young's modulus and relatively low cold compressive strength are indicative of the highly brittle nature of this material. From the composition it is evident that this material is primarily a homogeneous material. In this context, the presence of a highly dense continuous mode AE signal is indicative of a material failure due to continuous generation of a microcrack network similar to that occurring in glass.

The time domain AE signals for the bauxite material representing points a to f are embedded in Fig. 11. The time domain signal corresponding to point a representing region I of Fig. 11 is predominantly of a burst emission type. Points c and f representing region II of Fig. 11 for bauxite material are also burst-type signals but with higher density. Points d and e, representing region III of Fig. 11, are predominantly burst-type signals similar to point a. This indicates that, owing to its high compressive strength, the material removal occurring in the bauxite material is primarily of the transgranular fracture type. Region II of Fig. 11 consists of material removal from the soft matrix and region III represents material removal through transgranular fracture of hard inclusions.

Frequency decomposition of the ARMA model representing the AE signals was performed to gain a better understanding of the physics of the material removal process in AWJ drilling. Tables 3, 4 and 5 show the results of the frequency decomposition of magnesia chromite, sintered magnesia and bauxite respectively. The tables indicate the primary and secondary roots of the ARMA models representing each data set.

From Table 3 it can be seen that all the primary roots are complex which denote an exponentially decaying dynamic model. It can also be seen that the power of the primary

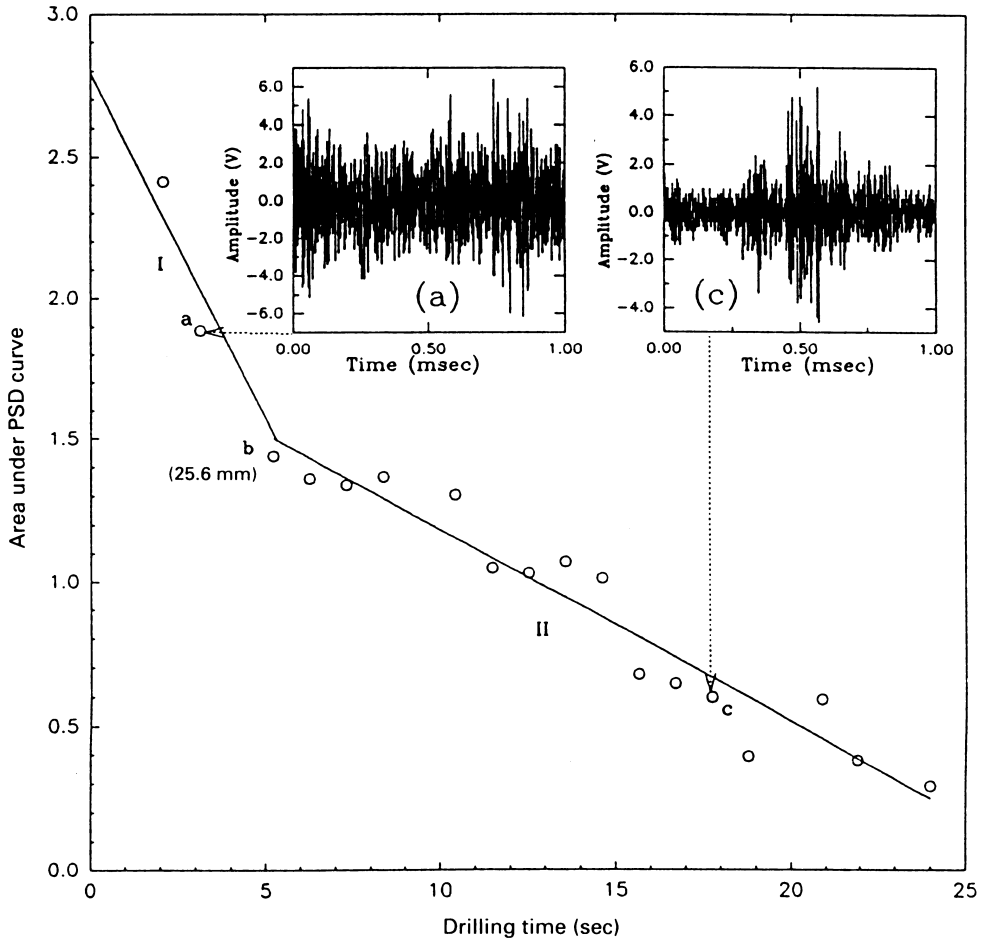

Fig. 10 Area under PSD curve versus drilling time (sintered magnesia)

root reduces and that of the secondary root increases gradually until the critical depth (point b of Fig. 9) is reached. The frequency range of the primary root is 120–160 kHz, whereas most of the secondary frequencies are observed to be in the range of 70–180 kHz. The impinging jet can be considered to be responsible for the primary root and the rebounded jet can be considered to be responsible for the secondary root since the impinging jet has higher power than the rebounded jet. The above trend indicates that with progressive depth of drilling, the effect of the impinging jet reduces and that of the rebounded jet increases. Beyond the critical depth, the presence of the rebounded jet in the narrow hole creates turbulence and hence affects the penetration process. The damping effect of the rebounded jet is also indicated by the negative power of the secondary root at larger depths and the presence of negative real roots.

In the case of sintered magnesia (Table 4) all the primary roots and almost all the secondary roots are complex. The frequency and power of the primary root reduce and those of the secondary root increase gradually until the critical depth (point b of Fig. 10) is reached. Beyond the critical depth the power of the secondary frequency increases further, such that there is a switch between the primary and the secondary root. The primary frequency after the critical depth are observed to be in the range of 200–330 kHz, whereas the secondary frequency is in the range of 140–180 kHz. This frequency range is different from that observed in the case of magnesia chromite. The presence of the negative power of the secondary frequency and the frequency shift at higher depths indicate the increased damping effect of the rebounded jet.

For bauxite (Table 5) the primary frequency is observed to be in the range of 120–200 kHz for all depths, whereas the secondary frequency is in the range of 60–90 kHz until a depth of 40 mm is reached. Beyond a 40 mm depth the secondary frequency increases gradually. This increase in the secondary frequency indicates an increased damping effect at larger depths. This trend in the bauxite material also supports the view that the primary frequency is caused by the impinging jet and the secondary frequency is caused by the rebounded jet. However, the presence of a failure mode due to transgranular fracture produces a combination of weak and strong signals from the soft matrix and hard inclusions respectively. This is responsible for the lack of a clear trend in the power of the roots with drilling depth.

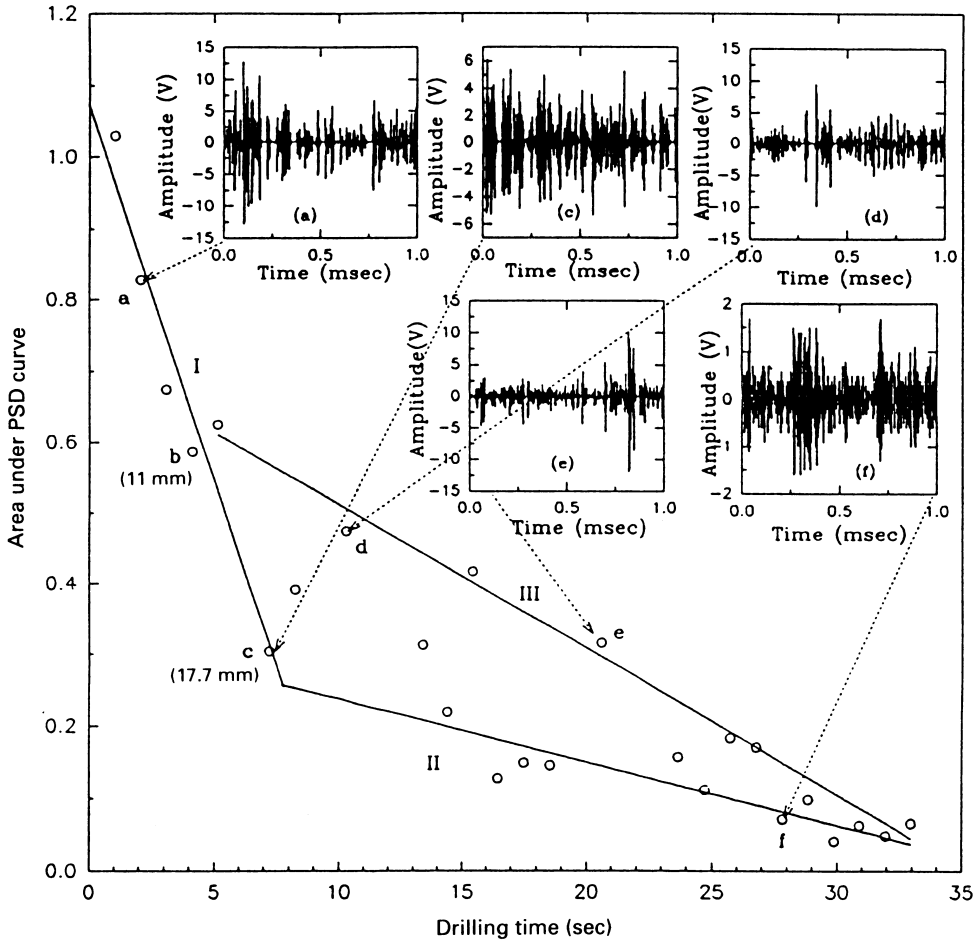

Fig. 11 Area under PSD curve versus drilling time (bauxite)

4 CONCLUSIONS

The acoustic emission sensing technique provides critical information about the material removal mechanisms in the AWJ drilling process. Material removal in ceramic materials characterized by hard inclusions in a much softer matrix is primarily due to intergranular erosion indicated by sparse continuous AE. The material removal in highly brittle materials in AWJ drilling is primarily due to continuous propagation of a microcracking network as indicated by dense continuous AE. Material failure in high compressive strength materials is caused by transgranular fracture indicated by a predominantly burst emission signal.

AE signal amplitude is about three to four times higher during the pure water jet impingement stage than during drilling. Material removal rate and penetration rate studies indicate that the back flow of the jet has sufficient kinetic energy to remove material from the walls of the drilled hole in the case of the materials under study causing hole divergence. Both material removal rate and penetration rate decrease with an increase in material compressive strength. Decrease in penetration rate and increase in damping effect caused by jet turbulence are responsible for the reduction in the AE signal amplitude with progressive drilling time.

AE_{RMS} is a promising tool for on-line monitoring of the depth of AWJ drilling. Stochastic modelling of AE signals has provided an insight into the physics of the AWJ drilling process. The area under the PSD curve exhibits the same trend as the penetration rate. For each material, the impinging jet is the dominant AE source until a critical depth beyond which the damping effect of the rebounded jet becomes significant. Frequency decomposition of the ARMA models suggests that the primary frequency of the AE signal is caused by the impinging jet and the secondary frequency is caused by the rebounded jet.

Table 3 Frequency decomposition—magnesia chromite

Time (s)	Depth (mm)	Root*	Discrete Real	Discrete Imaginary	Frequency (MHz)	Power (%)
0.85	9.57	1	0.5204	±0.6172	0.1385	80.10
		2	0.7901	±0.3851	0.0722	19.90
1.70	17.37	1	0.5026	±0.6693	0.1475	78.62
		2	0.8119	±0.3846	0.0704	21.38
2.55	23.73	1	0.4938	±0.6766	0.1497	55.14
		2	0.8142	±0.4418	0.0791	44.86
3.40	28.92	1	0.7539	±0.5087	0.0945	51.50
		2	0.4556	±0.7412	0.1623	48.50
5.10	36.59	1	0.5276	±0.6447	0.1408	99.12
		2	−0.5842	±0.3528	0.4135	0.88
6.80	41.70	1	0.4950	±0.7663	0.1587	65.4
		2	0.8020	±0.4740	0.1132	34.6
7.65	43.57	1	0.5619	±0.7144	0.1439	98.72
		2	−0.3328	±0.0000	0.1751	1.28
8.50	45.10	1	0.534	±0.7354	0.1501	94.08
		2	−0.0610	±0.0000	0.4451	5.92
9.35	46.34	1	0.6109	±0.5783	0.1206	126.78
		2	0.2760	±0.6249	0.1838	−26.78
10.2	47.36	1	0.4986	±0.7606	0.1577	94.76
		2	−0.2204	±0.0000	0.2407	5.24
11.5	48.20	1	0.5544	±0.5856	0.1294	155.88
		2	0.1761	±0.3849	0.1817	−55.88

* 1, primary; 2, secondary.

Table 4 Frequency decomposition—sintered magnesia

Time (s)	Depth (mm)	Root*	Discrete Real	Discrete Imaginary	Frequency (MHz)	Power (%)
2.08	12.68	1	0.19639	±0.5471	0.1951	96.36
		2	−0.8960	±0.0000	0.0175	3.63
3.13	17.76	1	0.4592	±0.6358	0.1505	63.82
		2	0.1917	±0.0000	0.2629	36.18
5.21	25.95	1	0.5308	±0.6781	0.1443	50.14
		2	−0.4020	±0.5925	0.3449	40.50
6.26	29.23	1	−0.3757	±0.5416	0.3465	56.96
		2	0.4978	±0.6374	0.1445	33.20
7.30	32.07	1	−0.1251	±0.6525	0.2801	52.20
		2	0.5282	±0.6829	0.1452	41.32
8.35	34.52	1	−0.2247	±0.6645	0.3162	71.76
		2	0.5082	±0.7706	0.1572	28.24
10.4	38.48	1	−0.0032	±0.6585	0.2508	79.14
		2	0.5018	±0.7746	0.1585	20.86
11.5	40.07	1	−0.0565	±0.6017	0.2649	68.74
		2	0.4792	±0.7386	0.1584	31.26
12.5	41.44	1	−0.3335	±0.5255	0.3400	59.36
		2	0.4521	±0.6564	0.1540	30.58
13.6	42.62	1	−0.1043	±0.7330	0.2725	79.52
		2	0.4940	±0.7341	0.1557	20.48
14.6	43.64	1	−0.0358	±0.6530	0.2587	82.46
		2	0.4925	±0.7129	0.1538	17.54
15.7	44.53	1	0.0194	±0.6826	0.2455	80.28
		2	0.4861	±0.7400	0.1575	19.72
16.7	45.30	1	−0.1878	±0.6277	0.2963	76.32
		2	0.5120	±0.7282	0.1525	23.68
17.7	45.96	1	−0.1477	±0.6079	0.2879	74.68
		2	0.4924	±0.6660	0.1487	25.32
18.8	46.53	1	0.0788	±0.5272	0.2264	138.08
		2	−0.3230	±0.0000	0.1799	−38.08
19.8	47.03	1	0.1571	±0.4975	0.2013	115.16
		2	−0.5404	±0.0000	0.0979	−15.16
20.9	47.45	1	−0.3157	±0.6424	0.3227	66.16
		2	0.4388	±0.7477	0.1655	33.84
21.9	47.82	1	−0.0977	±0.6747	0.2729	72.52
		2	0.4703	±0.7429	0.1602	27.48
24.0	48.42	1	−0.2974	±0.5817	0.3252	73.00
		2	0.4816	±0.7138	0.1555	13.00

* 1, primary; 2, secondary.

ACKNOWLEDGEMENTS

This work is supported by National Science Foundation (DMI-9523010), Center for Manufacturing Systems, University of Kentucky, Lexington, Kentucky, The University of Tulsa, Tulsa, Oklahoma, and Flow International Inc., Kent, Washington.

REFERENCES

1 **Kovacevic, R., Hashish, M., Mohan, R. S., Kim, T. J., Ramulu, M.** and **Geskin, E. S.** State of the art of research and development in abrasive water jet machining. *Trans. ASME, J. Mfg Sci. Engng*, 1997, **119** (4B), 776–785. 75th Anniversary Issue.

2 **Hashish, M.** Turning, milling, and drilling with abrasive water jets. In Ninth International Symposium on *Jet Cutting Technology*, Japan, October 1988, pp. 113–131.

3 **Savanick, G. A.** and **Krawza, W. G.** An abrasive water jet rock drill. In Proceedings of Fourth US Water Jet Conference, August 1987, pp. 129–132.

4 **Hashish, M.** The potential of an ultrahigh-pressure abrasive water jet rock drill. In Fifth American Water Jet Conference, Canada, August 1989, pp. 321–332.

5 **Hashish, M.** and **Whalen, J.** Precision drilling of ceramic-coated components with abrasive-waterjets. *Trans. ASME, J. Engng Gas Turbines and Power*, 1992, **115**, 148–154.

6 **Raju, S. P.** and **Ramulu, M.** A transient model for material removal in the abrasive water jet machining process. In Proceedings of Seventh American Water Jet Conference, Seattle, Washington, August 1993, pp. 141–155.

7 **Frye, R. W.** and **Polk, D. H.** Laser drilling of ceramic for heat exchanger applications. In Proceedings of International

Table 5 Frequency decomposition—bauxite

Time (s)	Depth (mm)	Root*	Discrete		Frequency (MHz)	Power (%)
			Real	Imaginary		
1.03	2.99	1	0.4644	±0.5844	0.1431	65.56
		2	0.7676	±0.4333	0.0818	34.44
2.06	5.81	1	0.4775	±0.6162	0.1451	78.2
		2	0.7705	±0.4049	0.0770	21.8
3.09	8.47	1	0.4606	±0.5756	0.1426	70.68
		2	0.7719	±0.4130	0.0782	29.32
4.12	10.99	1	0.4991	±0.5986	0.1394	102.34
		2	0.7374	±0.3698	0.0739	−2.34
5.15	13.37	1	0.4826	±0.6277	0.1457	88.68
		2	0.7719	±0.3797	0.0728	11.32
7.21	17.74	1	0.5565	±0.6708	0.1398	100.0
8.24	19.75	1	0.3865	±0.6041	0.1594	51.18
		2	0.7576	±0.4815	0.0901	48.82
10.3	23.44	1	0.5055	±0.6944	0.1498	100.0
13.4	28.25	1	0.4575	±0.5339	0.1372	64.04
		2	0.7743	±0.4059	0.0768	35.94
14.4	29.68	1	0.4445	±0.5859	0.1467	70.40
		2	0.7930	±0.4672	0.0847	40.82
15.5	31.03	1	0.4535	±0.5736	0.1435	70.50
		2	0.7697	±0.4141	0.0786	29.50
16.5	32.30	1	0.5130	±0.6684	0.1458	100.0
17.5	33.51	1	0.4821	±0.6156	0.1442	84.26
		2	0.7829	±0.3420	0.0656	15.74
18.5	34.65	1	0.5050	±0.5841	0.1365	101.96
		2	0.7755	±0.3128	0.0610	−1.96
20.6	36.74	1	0.5616	±0.5752	0.1269	111.34
		2	0.7584	±0.3097	0.0617	−11.34
23.7	39.47	1	0.3395	±0.6653	0.1749	65.0
		2	0.7815	±0.4279	0.0797	35.0
24.7	40.28	1	0.4386	±0.6909	0.1608	99.86
		2	−0.6597	±0.0000	0.0662	0.28
25.8	41.05	1	0.3638	±0.6806	0.1724	59.22
		2	0.6032	±0.5839	0.1224	40.78
26.8	41.77	1	0.2311	±0.6899	0.1986	61.78
		2	0.6434	±0.5744	0.1160	38.22
27.8	42.46	1	0.6418	±0.6285	0.1233	76.54
		2	0.0712	±0.7185	0.2343	23.46
28.8	43.11	1	0.6641	±0.6171	0.1192	75.28
		2	0.1280	±0.5414	0.2131	20.78
29.9	43.72	1	0.6285	±0.6025	0.1216	53.64
		2	0.2835	±0.6610	0.1855	46.36
30.9	44.29	1	0.5870	±0.6541	0.1336	103.36
		2	0.0366	±0.6407	0.2409	−3.36
31.9	44.84	1	0.6095	±0.6536	0.1306	84.92
		2	0.1285	±0.7152	0.2217	15.08
32.9	45.35	1	0.5763	±0.6561	0.1353	84.0
		2	0.0817	±0.6888	0.2312	16.0

*1, primary; 2 secondary.

Conference on *Applications of Lasers and Electro-Optics*, Ohio State University, Ohio, 1986, pp. 137–144.

8 **Mohan, R., Momber, A.** and **Kovacevic, R.** On-line monitoring of depth of AWJ penetration using acoustic emission technique. In *Water Jet Cutting Technology*, 1995, pp. 649–664 (Mechanical Engineering Publication, Suffolk).

9 **Liu, J. J.** and **Dornfeld, D. A.** Monitoring of micro-machining process using acoustic emission. *Trans. NAMRI/SME*, 1992, **XX**, 189–195.

10 **Blum, T.** and **Inasaki, I.** A study on acoustic emission from the orthogonal cutting process. *ASME, J. Engng for Industry*, 1990, **112**, 203–211.

11 **Emel, E.** and **Kannatey-Asibu, E.** Acoustic emission monitoring of the cutting process negating the influence of varying conditions. *Trans. ASME, J. Engng Mater. Technol.*, 1991, **113**, 456–464.

12 **Sturges, R. H.** Monitoring milling processes through AE and tool/part geometry. *Trans. ASME J. Engng for Industry*, 1992, **114**, 8–14.

13 **Pandit, S. M.** and **Stacey, J. D.** Data dependent system analysis of acoustic emission in grinding. *ASME PED*, 1993, **64**, 437–444.

14 **Chryssolouris, G., Sheng, P., Anastasia, N.** and **Domroese, M.** Investigation of acoustic sensing for laser drilling. *Trans. NAMRI/SME*, 1992, **XX**, 227–233.

15 **Momber, A., Mohan, R.** and **Kovacevic, R.** Acoustic emission measurements on brittle materials during abrasive water jet cutting. In First International Machining and Grinding Conference, 1995, paper MR 95-184, pp. 439–458.

16 **Schofield, B. H.** Research on the sources and characteristics of acoustic emission. *ASTM STP 505*, 1972, pp. 11–19.

17 **Kovacevic, R.** and **Zhang, Y. M.** Identification of surface characteristics from large samples. *Proc. Instn Mech. Engrs, Part C, Journal of Mechanical Engineering Science*, 1992, **206**, 275–284.

18 **Pandit, S. M.** and **Wu, S. M.** *Time Series and Systems Analysis with Application*, 1983 (John Wiley, Reprinted by Krieger Publishing, Melbourne, Florida).

19 **Pandit, S. M.** and **Shunmugam, M. S.** Signature of machine tool errors on surface texture by DDS. *Trans. ASME, J. Engng for Industry*, 1992, **114**, 370–374.

